V-shaped domain wall probes for calibrated magnetic force microscopy

R. Puttock[1,2], H. Corte-León[1,2], V. Neu[3], D. Cox[1,4], A. Manzin[5], V. Antonov[2], P. Vavassori[6,7], and O. Kazakova[1]

[1]National Physical Laboratory, Teddington, TW11 0LW, UK
[2]Physics Department, Royal Holloway University of London, Egham, TW20 0EX, UK
[3]Leibniz Institute for Solid State and Materials Research, Dresden, 01069, Germany
[4]Advanced Technology Institute, University of Surrey, Guildford GU2 7XH, United Kingdom
[5]Istituto Nazionale di Ricerca Metrologica, Torino, I-10135, Italy
[6]CIC nanoGUNE, San Sebastián, E-20018, Spain
[7]IKERBASQUE, Basque Foundation for Science, Bilbao, 48013, Spain

Abstract— **Magnetic force microscopy qualitatively resolves stray magnetic fields, but its fundamental flawed include limited quantitative analysis, and difficulties in measuring samples with heterogeneous magnetic areas. We propose a custom-made domain wall probe (DWP) with a *V*-shaped magnetic nanostructure on one face of a non-magnetic probe; which behaves as a low moment probe with high coercivity to reduce magnetic switching in the presence of strong stray fields. The performance of the DWP is compared against commercial probes in its ability to resolve striped domain structures of a thin reference film. The reference sample is also used to calibrate the three probes by acquiring the tip-transfer function (TTF) from a Fourier transform approach. The calculated TTF is used to predict the MFM response from a thin nanostructure with a different magnetization structure to the film and compared to experimental results.**

Index Terms – **domain wall probes, magnetic force microscopy, magnetic probe calibration, quantitative MFM, tip-transfer function**

I. INTRODUCTION

Conducting reliable quantitative measurements of spatially resolved magnetic fields on the nanoscale is beneficial for a number of industries, ranging from automobile manufacture [1] to bio-medicine [2]. Although such measurements are available on a macroscopic scale, a universal calibration method for measuring nanomagnetic properties remains unresolved. A number of approaches have been reported in recent years such as superconducting quantum interference devices [3], or nano-Hall sensors [4]; however, they often require time-consuming sample preparation or specialized methods of operation [5].

For these reasons, magnetic force microscopy (MFM) is well placed to quantitatively determine nanoscale magnetic fields due to the technique's high spatial resolution (<10 nm) [6], ease of use in standard conditions, and high abundance in research and industrial environments. Methods involving nanoscale coils [7], Hall sensors [8] and electron holography [9] are some of many proposed in literature to calibrate magnetic probes. However, MFM is still considered a qualitative technique as probe dimensions and properties wildly vary within and between commercial batches, and calibration values for the same probe can vary depending on the dimensions of samples being studied [7], [10].

Here we use a calibration technique based on imaging a reference film with a strong perpendicular magnetic anisotropy (PMA) and well known parameters such as domain shape, magnetization saturation and anisotropy constant. Using the reference film and a fast Fourier transform (FFT) approach, it is possible to extract the tip-transfer function (TTF), which describes the properties of an MFM probe without any assumptions of its geometry or magnetization [11], [12]. From a probe's TTF, micromagnetic simulations of other thin samples can be produced, thus predicting the MFM response of a sample by the probe is possible. Comparable physical results between MFM responses *in silico* and from physical measurement is the ultimate test for a validated calibration technique.

The TTF model is assessed by calibrating different probes and simulating their response when imaging a permalloy (Py) nanostructure. The probes studied are two commercially available probes, and a custom-made domain wall probe (DWP), which has a *V*-shaped magnetic nanostructure on a single face of the probe's pyramidal tip.

The probe's nanostructure behaves similarly to other cornered ferromagnetic architectures [13] - [15]). Thus the probe is expected to behave as a low moment probe from it localized stray field at the probe apex; but with a higher coercivity due to its thicker magnetic coating and shape. This probe was selected as the field distribution from a DW it is expected to be different to the stray field of commercial probes, and thus represents a greater challenge for the TTF approach.

The DWP's magnetic properties are compared against two commercial probes: a Nanosensor PPP-MFMR standard moment probe (SMP), from which the custom probe was fabricated; and an NT-MDT MFM_LM low moment probe (LMP), which is designed to image soft magnetic samples. Throughout the present work the quantification of spatial resolution and sensitivity is discussed from a number of methods. This includes introducing a simplistic method to quantify resolution for different probes and comparing with established techniques (i.e. TTF and the edge spread function). These methods can be performed from the same images of the reference film, thus providing useful insights for probe's properties without the use of mathematically and experimentally complex methods [16], [17].

II. EXPERIMENTAL

A. Probe Fabrication

DWPs were fabricated using commercially available probes (Nanosensors™ PPP-MFMR AFM [18]) by Ga-etching the magnetic CoCr coating [19] (thickness (t) = ~30 nm) with a focused ion beam (FIB) system; forming a V-shape structure on one face of the pyramidal tip. Figure 1 is an SEM image of a DW probe with the lithographed V-shape (a) and a schematic drawing (b). The nanostructure's arms are 7.78 µm in length by 400 nm in width, and they meet at ~40º.

B. Reference and Test sample

The reference sample is a sputtered $[Co(0.4nm)/Pt(0.9nm)]_N$ multilayer where N=100 [20]. The interface anisotropy of the Co/Pt interfaces provides a perpendicular magnetic anisotropy of K = 0.52 MJ/m^3 which competes with the shape anisotropy of the thin film, Thus the magnetization collapses into a multi-domain state at remanence, forming the well-known labyrinth pattern with neighboring up and down domains. The domain width has an average value of 180 nm but due to a domain transition width of ~20 nm and the non-regularity of the domain arrangement, the sample contains lateral features from about 20 nm up to the scan size of 5 µm.

An L-shaped Py nanostructure, of t = 25 nm and w = 100 nm was used to validate the TTF approach. It has areas with low/high stray field, with intense field at the structure's apex [21].

C. Measurement Techniques

Probes were magnetized *ex situ* with a Nd magnet (~0.4T) and standard two-pass tapping mode MFM was performed with the Dimension Icon scanning probe microscope (Bruker, Massachusetts, USA) to map the topography and magnetic distribution of the tested samples. The oscillation setpoint (A_s) for the first pass was 40 nm peak-to-peak, whereas and the free oscillation amplitude (A_f) was 50 nm (defined at 3.5 µm above the surface). For the second pass, the interleave amplitude (A_L) of 42 ± 1 nm was observed for all probes at a 25 nm lift height (h_L) above the surface. The 'true' lift height for MFM measurements was determined from the amplitude sensitivity by manually approaching the surface until signs of contact were seen from the scope. From this, h_L= 0 nm was defined and thus the total distance (d_{total}) and true lift height with respect to the surface was determined (i.e. $d_{total} = h_L + A_s$).

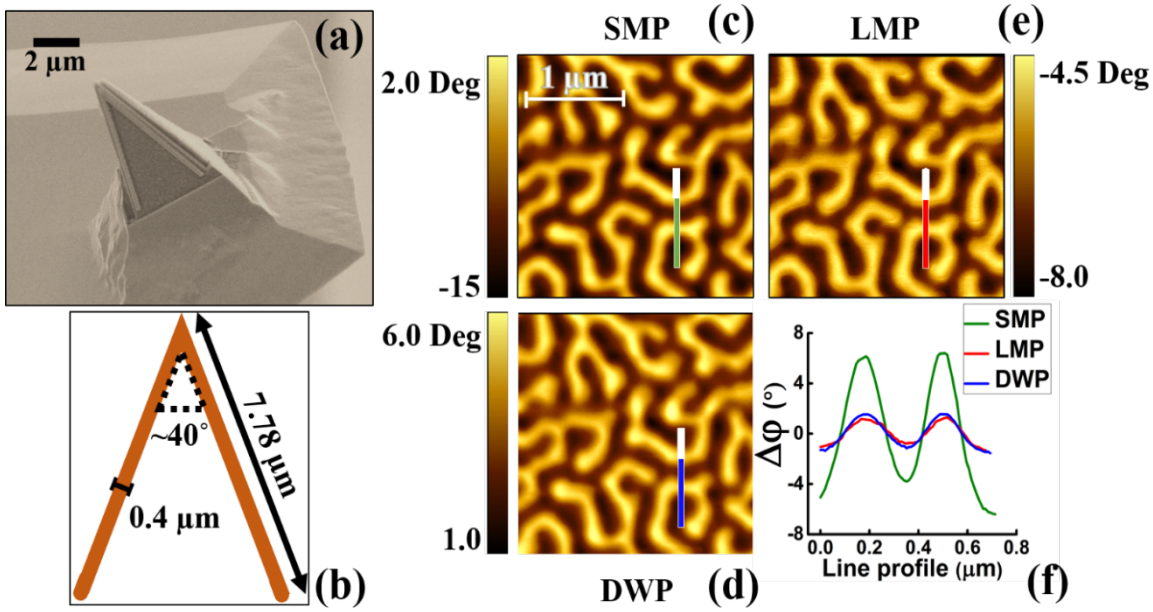

Figure 1. (a) SEM image of a DWP fabricated from a Nanosensor PPP MFMR probe. (b) Schematic diagram with the dimensions of the magnetic nanostructure. Magnetic force microscopy images of Co/Pt film in the same area (2.5×2.5 µm^2) with standard moment probe (c), domain wall probe (d) and low moment probe (e). Single pixel-width line profiles in locations indicated for all probes are displayed in f – note the phase changes have been offset at zero for easy comparison. White profiles represent the areas analyzed by edge spread function in section C.

The spring constants of the probes, used in the TTF calculations, were calculated from the tapping mode deflection sensitivity and thermal tuning. These were 4.001, 2.457 and 3.633 N/m for the SMP, LMP and DWP respectively.

All MFM visualization and data analysis were conducted with a combination of the Gwyddion (CMI, Brno, Czech Republic), and Origin Pro 2016 (OriginLab, Massachusetts, USA) software alongside programs written in-house with MATLAB® (MathsWorks Inc., Massachusetts, USA). The edge spread function was calculated from a custom plugin in the image processing software ImageJ (NIH, Maryland, US).

D. TTF and micromagnetic modelling

In the present implementation of the qMFM code the TTF describes the probe by quantifying its stray field derivative profile at d_{total} below the physical tip apex. The concept is based on the magnetostatic interaction between sample and probe, which can be expressed in Fourier space by multiplying the sample's effective magnetic surface charges and above defined TTF according to Eq. 1.

$$\frac{\partial F_z}{\partial z}(k) = -\sigma^*_{sample}(k) \cdot \frac{\partial H_z^{tip}}{\partial z}(k). \qquad (1)$$

For calculating the TTF, first the effective surface charge map of the reference sample is derived from the measured MFM image by considering the saturation magnetization value, domain transition width and film thickness. Then the TTF is computed in Fourier space by deconvolving the MFM image and surface charge map by means of the Wiener invert filter.

With a calibrated tip, the MFM signal of an arbitrary sample can be predicted quantitatively once the effective surface charge pattern is known. Here the Py nanostructure is used as a test sample as it possesses a completely different magnetization structure than the reference sample, and is still well defined. The spatial magnetization distribution was calculated with a parallelized micromagnetic solver [22], [23], which time-integrates the Landau-Lifshitz-Gilbert (LLG) equation by means of a norm-conserving scheme based on Cayley transform , and the magnetic volume charge ($\rho = div\vec{M}$) was subsequently computed. Due to the small film thickness (t_f) the surface charges can be approximated as t_f·ρ. This surface charge map is than convolved with the previously obtained TTF to produce a simulated MFM image, which is quantitatively compared with experiment.

III. RESULTS

A. Reference film characterization

The same 2.5×2.5 μm^2 area of the Co/Pt film was imaged with the two commercial probes and the DWP (Fig. 1 c-e). The SMP showed great ability to resolve domain structures and resulted in ~17˚ range in phase change (Δφ). This type of probe is used for measuring strong magnetic signals because of its thick coating and design (i.e. optimized spring constant, coercivity and remanent magnetization) [18]. From qualitative comparison the LMP image sharpness is reduced compared to the SMP image, and the range is significantly reduced, i.e. Δφ(LMP) = 0.19×Δφ(SMP) (as calculated from a full area histogram) demonstrating the LMP's smaller stray field.

Despite significantly reduced area of magnetic coating on the custom-made DWP, the quality of the image looks similar to the LMP, though with a miniscule reduction in sharpness. The line profiles in Fig. 1f appear near identical despite the differences in magnitude seen on the color scale, which indicates slightly higher sensitivity for the DWP. This is because the line profiles show a localized region which are coincidentally similar, but DWP has a significantly greater phase contrast across the globalized area, Δφ(DWP) = 0.29×Δφ(SMP). The comparable sensitivity despite less magnetic material can be attributed to the strong stray field generated by the domain wall on the probe and localized location of DW on the probe's apex. The thickness of the nanostructure accounts for the loss of coating area, when compared to the LMP, to give higher sensitivity.

Low moment probes have a tendency to switch magnetic orientation when imaging a highly magnetic samples such as the Co/Pt film. This can lead to distorted and inaccurate images (Fig. 2). All three images were taken with the same low moment probe but with different parameters: the left hand image is as seen in Fig. 1, no switching is observed; the central and right-hand images are the LMP with "software optimized" parameters, derived from the pre-set values in the program and parameters obtained from the frequency sweep, at 75 and 25 nm lift heights respectively.

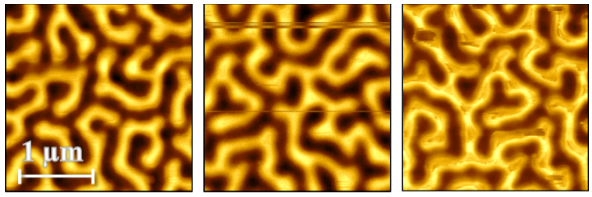

Figure 2. Low moment probe in manually optimized conditions to prevent switching (left), and automated parameters at 75 nm (center) and 25 nm (right) lift heights above the surface.

As has been shown throughout the present work, it is possible to image a film with large PMA from a commercial LMP, however to reduce chances of switching it requires manual optimized parameters, which is time consuming and specialized. Magnetic switching was not seen for the DWPs in any cases discussed, suggesting it is more reliable than LMP if imaging heterogeneously hard and soft magnetic samples. All further comparisons of probes are from the manually optimized conditions, as seen in Fig. 1,

including the non-switched LMP for a fairer quantification of magnetic properties.

B. Magnetic probe calibration

The TTFs for the three probes are summarized in Figure 3. As expected, the LMP has a stray field values reduced by about a factor of four compared to the SMP. But also the DWP has a similarly reduced TTF peak, classifying it as a low moment probe. The commercial probes are very symmetrical when comparing the *x* and *y* cross-sections, whereas the DWP is not. This is attributed to the presence of the DWP nanostructure on a single pyramidal face as opposed to the even four-sided coating of the commercial probes. As the TTF profile samples the magnetic charges on the sample surface during MFM measurement, the sharpness of the TTF peak is a qualitative measure of the probe's lateral resolution. When comparing the TTFs to their peak maximum, the LMP appears to possess the sharpest peak.

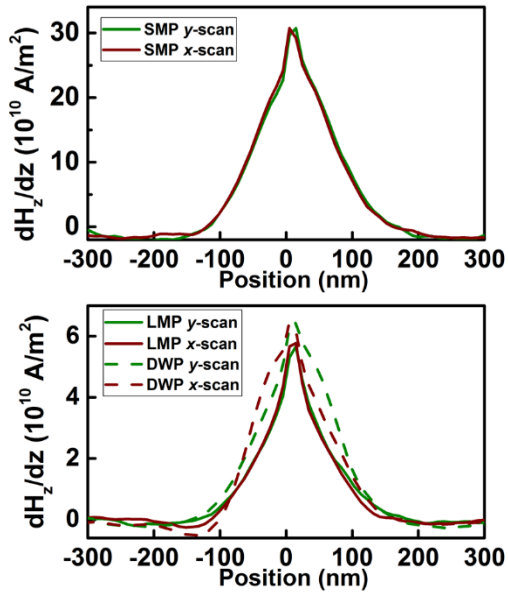

Figure 3. Cross-sectional plots of the real space tip-transfer function for standard moment (top), low moment (bottom solid) and domain wall probes (bottom dashed) in *x* and *y* directions (burgundy and green respectively).

C. One-dimensional statistical analysis

The resolution quality factor (R_s) is derived from separation chromatography, where it defines the separation of adjacent peaks with respect to their peak widths [24]. R_s is defined as:

$$R_s = \frac{x_{c2}-x_{c1}}{\frac{1}{2}(w_{b1}+w_{b2})} = 1.18 \times \frac{x_{c2}-x_{c1}}{w_{0.5h1}+w_{0.5h2}} \qquad (2)$$

where $x_{c2} - x_{c1}$ is the distance between peak maxima on the line profile, and *w* is the profile base full width (*b*) and full width at half maximum (*0.5h*) respectively. The two forms in equation (2) are equivalent, with the right hand form preferred for our purposes as the base width is less reliable.

Equation (2) is simple, thus ideal as a coarse test for lateral resolution, but it makes assumptions about the peak shapes; the adjacent peaks are Gaussian shaped and have the same areas and standard deviations. [25]. These assumptions are considered oversimplified for asymmetric peaks; however, the striped domains of this reference film are approximately the same widths and field strengths, thus the model can be considered relatively accurate. Although profiles from MFM images cannot be considered Gaussian, we have found Gaussian functions accurately fit the data-sets well enough for this statistical comparison.

Due to physical processes (e.g. signal attenuation) adjacent peaks are rarely fully resolved if they are near in proximity, leading to a reduction in maximum/minimum phase signals [Fig. 4a].

In Fig. 4 (b) and (c), we demonstrate the R_s method against the edge spread function (ESF), a simplistic ISO method which quantifies image sharpness based on line profile steepness ($D_{80\text{-}20}$), see Ref. [26]. The first trough to peak for line profiles in Fig. 1 (indicated in white) was used to calculate the ESF for all probes; the distance between points of defined intensities (20% to 80% is common) was used as a measure of sharpness [Fig. 4(c)]. The results are displayed in Table I.

Table I. Quantification of resolution from the peak resolution equation and edge spread function.

Probe	R_S ±2u (arb)	ESF ±2u (nm)
SMP	1.21 ± 0.04	70.8 ± 3.9
LMP	1.13 ± 0.12	70.1 ± 4.4
DWP	1.16 ± 0.06	65.8 ± 3.1

Qualitatively, it appeared that the SMP image was the most resolved, whereas the two other images were more similar. These observations were well reflected in the quantitative results from the R_s calculation, but not in the ESF, which ranked the DWP as the sharpest profile ($D_{80\text{-}20}$ = 65.8 nm) and the SMP the shallowest. The ESF approach, due to its origin, uses the image files rather than the raw data, hence the arbitrary intensity units in Figure 4c, however this should not affect the results providing a reasonable color scale was used in the visualization software.

Comparing the ESF with the TTF sharpness and the qualitative results, we can conclude the model is not a good statistical test for resolution from striped reference materials.

We demonstrate an example of both the qualities and limitations of the peak resolution method in Table I. In this example, the most common ranking order from the method is shown; produced from several line profiles in a 25 μm^2 scan area, though the numerical values do shift depending on the localized region. SMP was quantified as the sharpest from its larger R_s value, also seen in qualitative and TTF results (when considering TTF sharpness and magnitude). However, R_s contradicts the TTF by calculating the LMP is lower resolution than the DWP. This arises from worse fit for the LMP, as indicated by its larger expanded uncertainty (2*u*) in Table I.

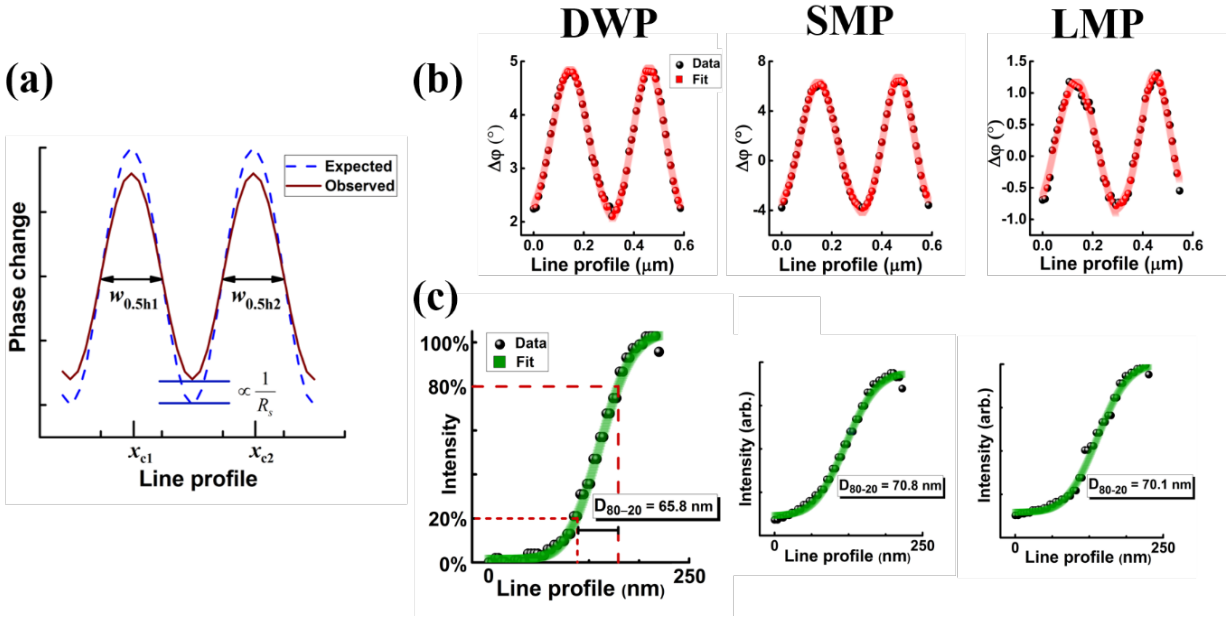

Figure 4. (a) Labelled schematic of the peak resolution method. (b) The data (black spheres) and fit (red line) of the line profiles from figure 1 for the domain wall (left), standard moment (center) and low moment (right) probes. (c) Edge spread function data (black spheres) and fit (green line) from white line profiles in Figure 1.

For a more meaningful demonstration of the fit we compared the adjacent R^2 values for the three line profiles; this quantifies the quality of the fit, with a perfect fit defined as $R^2 = 1$. For both SMP and DWP the R^2 indicates a good fit (both 0.997), however LMP was considerably worse $R^2 = 0.978$.

We conclude for a coarse test of resolution to use the R_s method over the ESF as it is simple and reliable for probe and/or parameter comparisons on the striped domain reference film. However, caution is advised and the R_s value should be qualified with an $R^2 \geq 0.99$. If R^2 is significantly lower the results are less conclusive and characterized by higher uncertainty.

D. Simulated MFM response

Fig. 5(a) is a color representation of the magnetization configuration in an angle plot for the Py structure with tail-to-tail magnetization and thus a head-on domain wall in the apex. Hence, a highly localized surface charge density is shown, as illustrated in Fig. 5(b). By convolving these charges with the three TTF results phase response expected from the MFM experiment can be calculated [Fig. 5(c)]. Due to the lateral extension of the TTF (several tens of nanometers) the contrast outside of the Py structure is also expected. The calculations predict a negative symmetrical phase shift at the corner of the L-shape; the absolute values are shown in the profiles [Fig. 5(e)].

Fig. 5(d) displays the measured MFM signal. Both LMP and DWP exhibit the expected negative peak in the localized region, and peak height and width compare remarkably well with the predicted equivalents [Fig. 5(e) right and left panels, respectively].

In the case of the DWP, the phase shift contrast appears physically "squeezed" to the outer boundary of the of the *L*-shape corner. This anomaly can arise

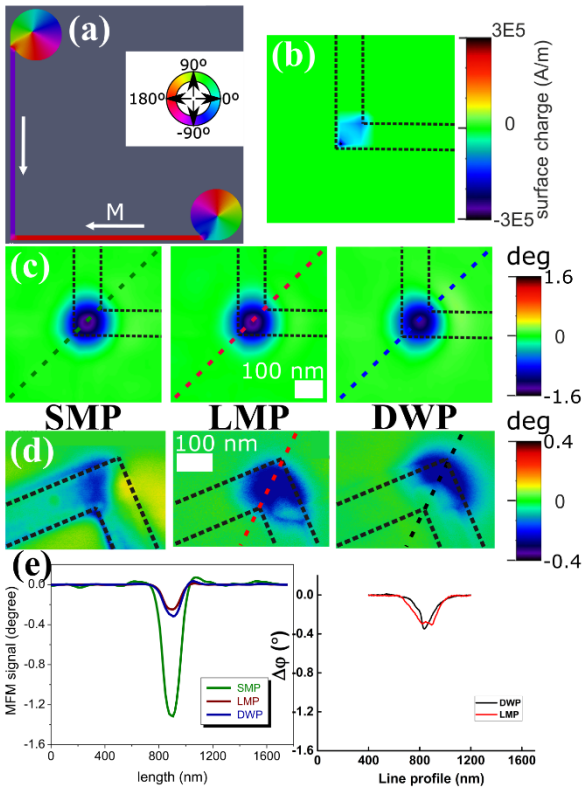

Figure 5. (a) Color representation of magnetization configuration for Py nanostructure. (b) Effective sample surface charge plot with large negative field at the L-shape's apex. (c) Simulated magnetic force microscopy images for standard moment, low moment and domain wall probe, alongside experimental results (d). (e) Simulated and experimental line profiles for the stated probes

from: 1) a probe asymmetry larger than derived from the reference measurement; 2) the probe's stray field interferes with the remanent domain state of the Py nanostructure.

The SMP contrast resembles an alternative stable remanent state without a DW at the L-shaped corner (see [13]). It is likely that the large stray field from the probe moves the domain wall away from the apex and the signal arises from magnetic flux bending around the corner. The experimental profile from SMP was excluded from 5(e) (left) for comparison. (blue dashed profile), and it is expectedly different to the simulated response. The profile shape is much more jagged due to the opposite contrasts in close proximity, with the second trough corresponding to nucleation around the inner corner of the L-shape opposed to the outer apex. This study is a prime example for the necessity of LMPs for imaging magnetic samples with low coercivity.

IV. CONCLUSION

We experimentally observe that the custom-made probe performs similarly to the commercial equivalents, behaving as a low moment probe with lower chance of magnetic switching *in situ*. The domain wall is clearly induced in a highly localized area at the nanostructure's apex; though initially predicted to improve resolution, we have demonstrated that this is not true for this design. Altering the geometry/dimensions of the nanostructure can be the subject of further study to improve the resolution. We have adopted a new method for simply and coarsely quantifying resolution with a reference film, and demonstrated it is more accurate than the ESF method for quantifying image sharpness; unlike the TTF, it does not require knowledge of reference sample's magnetization parameters. However, the success of the fit is imperative to the resolution quality factor. A failure to adhere can produce large uncertainty and reduces the reliability for comparison. TTFs further confirmed the similarity in sensitivity between the DWP and the LMP and revealed a higher lateral resolution for LMP than DWP. The asymmetry in the TTF for DWP demonstrated its ability to quantify uncommonly shaped probes alongside probes with more typical magnetic coating.

A reliable custom-made low moment probe for heterogeneous magnetic samples was demonstrated by comparing its properties with those exhibited by equivalent commercial standard and low moment probes. The custom-probe has a relatively high coercive field for a low moment probe due to its thickness and shape, thus reducing the magnetic switching seen whilst imaging hard magnetic samples. From resolution calculations and the TTF method discussed we have demonstrated the DWP has similar attributes to the LMP, and both are dissimilar to SMP in terms of magnetic sensitivity and stray field size. The TTF method was applied by predicting the MFM response by all tested probes for a permalloy structure. Due to reference film's considerably higher coercivity, the modelling for the SMP could not predict the perturbation of the head-on DW at the structure's apex. However, DWP and LMP simulations matched the experimental results with remarkable accuracy. Thus concluding the TTF method is an applicable calibration technique, providing the correct probe and/or reference material is selected for calibrated measurement of a test sample.

ACKNOWLEDGEMENT

This work was supported by EMPIR and EMPIR participating countries under Project S01 (NanoMag). The work of P. Vavassori was supported in part by the Basque Government under Project PI2015_1_19 and by the Spanish Ministry of Economy and Competitiveness under Project FIS2015- 64519-R (MINECO/FEDER).

IV. REFERENCES

[1] C. P. . Treutler, "Magnetic sensors for automotive applications," *Sensors Actuators A Phys.*, vol. 91, no. 1–2, pp. 2–6, Jun. 2001.

[2] T. Zhu, P. Chen, Q. H. Zhang, R. C. Yu, and B. G. Liu, "Giant linear anomalous Hall effect in the perpendicular CoFeB thin films," *Appl. Phys. Lett.*, vol. 104, no. 20, 2014.

[3] D. Vasyukov, Y. Anahory, L. Embon, D. Halbertal, J. Cuppens, L. Neeman, A. Finkler, Y. Segev, Y. Myasoedov, M. L. Rappaport, M. E. Huber, and E. Zeldov, "A scanning superconducting quantum interference device with single electron spin sensitivity," *Nat. Nanotechnol.*, vol. 8, no. 9, pp. 639–644, 2013.

[4] L. Di Michele, C. Shelly, J. Gallop, and O. Kazakova, "Single particle detection: Phase control in submicron Hall sensors," *J. Appl. Phys.*, vol. 108, no. 10, 2010.

[5] S. Porthun, L. Abelmann, and C. Lodder, "MFM of thin film media for high density magnetic recording.pdf," *J. Magn. Magn. Mater.*, no. 182, pp. 238–273, 1998.

[6] X. Li, W. Lu, Y. Song, Y. Wang, A. Chen, B. Yan, S. Yoshimura, and H. Saito, "Quantitatively probing the magnetic behavior of individual nanoparticles by an AC field-modulated magnetic force microscopy.," *Sci. Rep.*, vol. 6, p. 22467, Jan. 2016.

[7] T. Kebe and A. Carl, "Calibration of magnetic force microscopy tips by using nanoscale current-carrying parallel wires," *J. Appl. Phys.*, vol. 95, no. 3, pp. 775–792, 2004.

[8] Ó. Iglesias-freire, A. Lartsev, R. Yakimova, A. Asenjo, and O. Kazakova, "Magnetic Scanning Probe Calibration Using Graphene Hall Sensor," *IEEE Trans. Magn.*, vol. 49, no. 7, pp. 3520–3523, 2013.

[9] G. Matteucci, B. G. Frost, and F. F. Medina, "Study of the field around magnetic force microscopy probes using electron holography," *Ultramicroscopy*, vol. 99, no. 2–3, pp. 95–102, 2004.

[10] S. Vock, F. Wolny, T. Mühl, R. Kaltofen, L. Schultz, B. Büchner, C. Hassel, J. Lindner, and V. Neu, "Monopolelike probes for quantitative magnetic force microscopy: Calibration and application," *Appl. Phys. Lett.*, vol. 97, no. 25, pp. 10–13, 2010.

[11] H. J. Hug, B. Stiefel, P. J. A. van Schendel, A. Moser, R. Hofer, S. Martin, H.-J. Güntherodt, S. Porthun, L. Abelmann, J. C. Lodder, G. Bochi, and R. C. OHandley, "Quantitative magnetic force microscopy on perpendicularly magnetized samples," *J. Appl. Phys.*, vol. 83, no. 11, pp. 5609–5620, 1998.

[12] S. Vock, Z. Sasvári, C. Bran, F. Rhein, U. Wolff, N. S. Kiselev, A. N. Bogdanov, L. Schultz, O. Hellwig, and V. Neu, "Quantitative magnetic force microscopy study of the diameter

evolution of bubble domains in a (Co/Pd)80 multilayer," *IEEE Trans. Magn.*, vol. 47, no. 10, pp. 2352–2355, 2011.
[13] H. Corte-León, V. Nabaei, A. Manzin, J. Fletcher, P. Krzysteczko, H. W. Schumacher, and O. Kazakova, "Anisotropic magnetoresistance state space of permalloy nanowires with domain wall pinning geometry.," *Sci. Rep.*, vol. 4, p. 6045, Aug. 2014.
[14] M. Donolato, M. Gobbi, P. Vavassori, M. Leone, M. Cantoni, V. Metlushko, B. Ilic, M. Zhang, S. X. Wang, and R. Bertacco, "Nanosized corners for trapping and detecting magnetic nanoparticles," *Nanotechnology*, vol. 20, no. 38, p. 385501, Sep. 2009.
[15] M. Precner, J. Fedor, J. Tobik, J. Soltys, and V. Cambel, "High resolution tips for switching magnetization MFM," *Acta Phys. Pol. A*, vol. 126, no. 1, pp. 386–387, 2014.
[16] S. V Kalinin, S. Jesse, B. J. Rodriguez, J. Shin, a P. Baddorf, H. N. Lee, a Borisevich, and S. J. Pennycook, "Spatial resolution, information limit, and contrast transfer in piezoresponse force microscopy.," *Nanotechnology*, vol. 17, no. 14, pp. 3400–3411, 2006.
[17] http://www. nanosensors. com/Poin.-P.-P.-M.-F.-M.-R.-C.-P.-M. Nanosensors, "Nanosensors," 2017. [Online]. Available: http://www.nanosensors.com/Point-Probe-Plus-Magnetic-Force-Microscopy-Reflex-Coating-afm-tip-PPP-MFMR. [Accessed: 17-Feb-2017].
[18] M. Jaafar, A. Asenjo, and M. Vázquez, "Calibration of coercive and stray fields of commercial magnetic force microscope probes," *IEEE Trans. Nanotechnol.*, vol. 7, no. 3, pp. 245–250, 2008.
[19] A. Manzin, V. Nabaei, H. Corte-León, O. Kazakova, P. Krzysteczko, and H. W. Schumacher, "Modeling of anisotropic magnetoresistance properties of permalloy nanostructures," *IEEE Trans. Magn.*, vol. 50, no. 4, pp. 1–4, Apr. 2015.
[20] S. Vock, C. Hengst, M. Wolf, K. Tschulik, M. Uhlemann, Z. Sasvári, D. Makarov, O. G. Schmidt, L. Schultz, and V. Neu, "Magnetic vortex observation in FeCo nanowires by quantitative magnetic force microscopy," *Appl. Phys. Lett.*, vol. 105, no. 17, 2014.
[21] A. Beguivin, H. Corte-León, A. Manzin, V. Nabaei, P. Krzysteczko, H. W. Schumacher, D. Petit, R. P. Cowburn, and O. Kazakova, "Simultaneous magnetoresistance and magneto-optical measurements of domain wall properties in nanodevices," *J. Appl. Phys.*, vol. 115, no. 17, p. 17C718, May 2014.
[22] O. Bottauscio and A. Manzin, "Parallelized micromagnetic solver for the efficient simulation of large patterned magnetic nanostructures," *J. Appl. Phys.*, vol. 115, no. 17, p. 17D122, May 2014.
[23] A. Manzin and O. Bottauscio, "A Micromagnetic Solver for Large-Scale Patterned Media Based on Non-Structured Meshing," *IEEE Trans. Magn.*, vol. 48, no. 11, pp. 2789–2792, Nov. 2012.
[24] A. Manzin and O. Bottauscio, "Connections between numerical behavior and physical parameters in the micromagnetic computation of static hysteresis loops," *J. Appl. Phys.*, vol. 108, no. 9, p. 93917, 2010.
[25] D. Harvey, *Modern Analytical Chemistry*. San Francisco: McGraw-Hill Companies, 2008.
[26] M. Dvořák, J. Svobodová, P. Dubský, M. Riesová, G. Vigh, and B. Gaš, "Equivalent peak resolution: Characterization of the extent of separation for two components based on their relative peak overlap," *Electrophoresis*, vol. 36, no. 5, pp. 646–654, 2015.
[27] BSI, *Surface chemical analysis — Fundamental approaches to determination of lateral resolution in beam-based methods*, First. BSI Standards Publication, 2013..
[28] S. Richard, D. B. Husarik, G. Yadava, S. N. Murphy, and E. Samei, "Towards task-based assessment of CT performance: system and object MTF across different reconstruction algorithms.," *Med. Phys.*, vol. 39, no. 7, pp. 4115–22, 2012.